# RIGA DYNAMO EXPERIMENT

*A. Gailitis*[1], *O. Lielausis*[1], *E. Platacis*[1], *G. Gerbeth*[2], *F. Stefani*[2]

[1] *Institute of Physics, University of Latvia, Miera 32, LV-2169 Salaspils, Latvia (gailitis@sal.lv)*

[2] *Forschungszentrum Rossendorf, P.O. Box 510110, D-01314 Dresden,Germany*

**Introduction.** Originally Riga dynamo experiment was devoted to demonstrate that enough strong and appropriately directed flow of fluid electroconductor can generate magnetic field very likely as Earth and other celestial bodies do. After the demonstrative goal was reached we went to study details such as field configuration in space and time. It appears that generation process is not completely regular. Apart from rigid rotation the field pattern execute complicate irregularities caused by turbulent nature of the sodium flow. There seems to be some similarity with annomalities and variations of the Earth magnetic field. The present paper deals with the details.

**1. Experiment setup.** The Earth field is generated in the liquid Earth core where thermal and sedimental convection exist in a form of long cyclonic/anticyclonic columns with helical stream inside (Fig. 1). They all together are supporting the Earth field. There are two successful experiments reproducing in labs something like. The Karlsruhe experiment reproduce the whole assemble of such columns. Our one works with only one separated column.

Two 100 kW motors 1 (Fig. 2) are driving a propeller which forces liquid sodium to circulate inside an annular vessel, part of which is located in the basement of sodium lab. The sodium flow is directed by two thin coaxial electroconducting cylindrical partition walls. In the central channel sodium is flowing down from the propeller. In the coaxial counter-flow channel the flow is upwards to the propeller. In an outer part of the vessel the sodium is moveless, it serves for electrical connection.

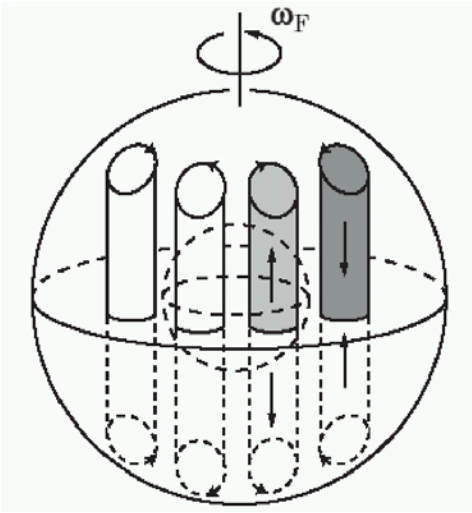


*Fig. 1.* Convection in the Earth core.

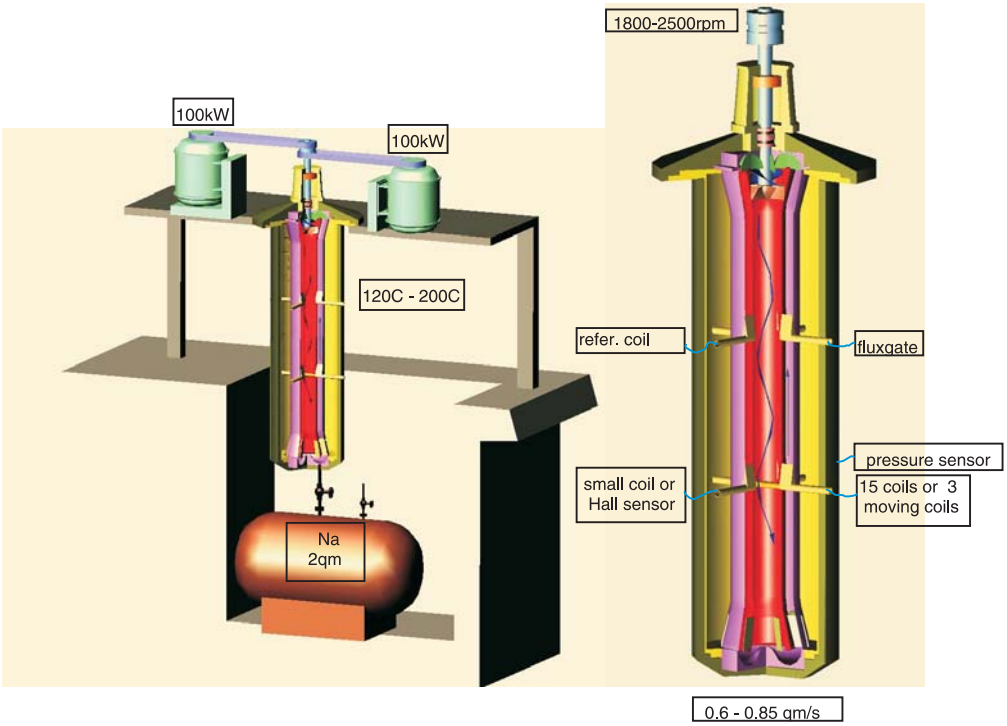


*Fig. 2.* Setup of the experiment.

Vanes located both before and after the propeller are designed to swirl the central flow as needed for field generation. The straight parts of channels are without any flow-guides. Hence the swirl is maintained by inertia only until the downstream end of the central channel and stopped by other vanes when the flow is being reversed.

Depending on sodium temperature the device starts to generate a magnetic field at propeller rotation rate of 1800 – 2000 rpm. The critical flow-rate is about 0.6 qm/s. The magnetic field pattern rotates round vertical axis hence any field sensor is feeling AC signal (Fig. 3). Sensor locations are shown on right part of Fig. 2.

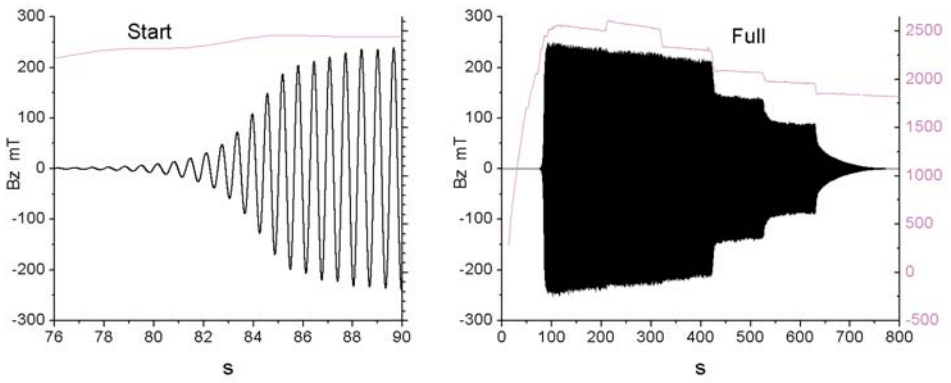


*Fig. 3.* One of fields records from the reference coil (Fig. 2).

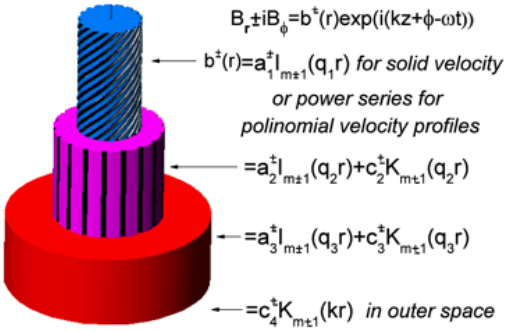


*Fig. 4.* Theoretical model.

**2. Theoretical background.** The design of the experiment was based on theoretical model consisting from three coaxial moving cylinders with ideal electrical contact on sliding surfaces (Fig. 4). Because of symmetry particular solutions of induction equation depend on axial distance $z$, azimuth $\varphi$ and time $t$ exponentially: $\exp(pt + ikz + im\varphi)$. In general the $k = k_r + ik_i$ and $p = p_r + ip_i$ are complex constants to be evaluated when the problem is solved. In our case $m = 1$. As far as cylinders are moving like rigid bodies the radial field dependence results in Bessel functions $I$ and $K$. Continuity of electric and magnetic fields on contact surfaces leads to a closed complex and transcendent (Bessel functions!) secular equation solved numerically (Fig. 5). Field vanishing on radial infinity is granted there by using only $K$ functions in the outer insulator.

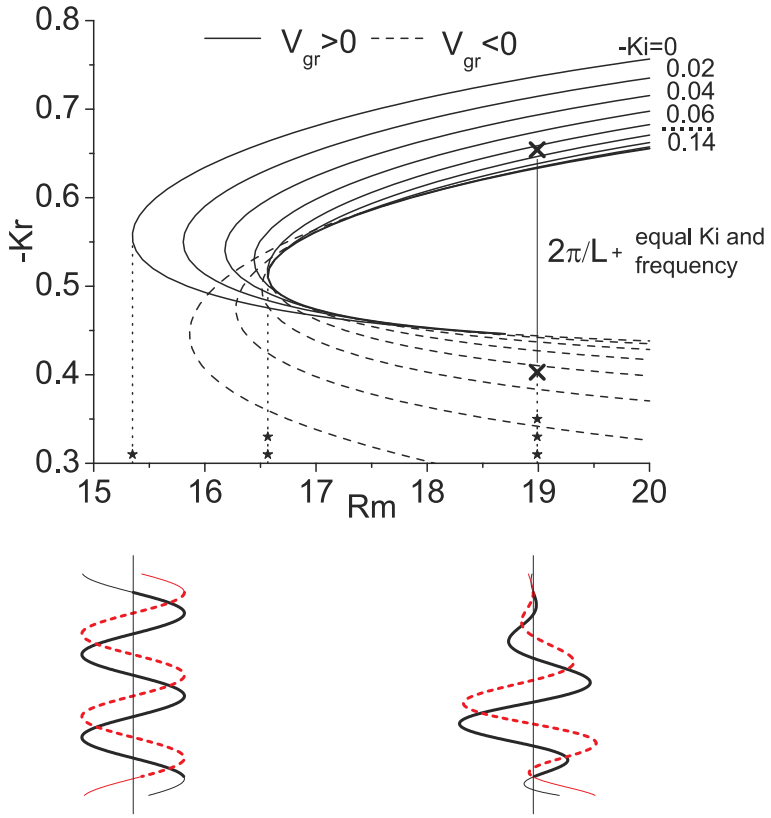


*Fig. 5.* Theoretical excitation curves.

Boundary conditions in $z$ direction are more complicate. For long model it is enough to demand zero axial current at two endpoints $z = \pm L/2$. Hence two solutions with equal $p$ and $k_i$ are needed. Temporary raising ($p_r = +0$) solutions exist for all Rm over $\mathrm{Rm}^*$ (marked by one star on Fig. 5). But between $\mathrm{Rm}^*$ and $\mathrm{Rm}^{**}$ for each $p$ and $k_i$ is only one solution. The two solutions can be found only beyond branching point $\mathrm{Rm}^{**}$. So $L = 2\pi/\delta k$ is the length of the model where the two mode superposition can fit in and $\mathrm{Rm}^{***}$ is the generation threshold at that length.

Three comments. First – water tests show flow in the central channel having velocity profiles different from rigid ones. No problem to replace $I$ functions there by power series derived from the induction equation using polynomial fits for the profiles. This was done when Fig. 5 was prepared. Second – location of $\mathrm{Rm}^{**}$ and $\mathrm{Rm}^{***}$ strongly depend on velocity in the reverse flow hence on its size. The $\mathrm{Rm}^{**}$ and $\mathrm{Rm}^{***}$ are raising to infinity when the return flow disappears. Because of this the channel sizes were optimized for minimum of $\mathrm{Rm}^{***}$. Third – our approach is only asymptotically true for long model. For limited length the two $k$ values considerably differ hence the zero conditions are fulfilled not on the whole end surface but only on some points there. Nevertheless our experiment was designed after asymptotic approach and it works very like as expected.

## 3. Magnetic field properties.

*3.1. 3.1 Instruments.* In our experiment magnetic field depend on propeller rotation rate, sodium temperature and on place where it is measured. Before and after experiment our device is in the Earth field deformed by building and steel frame: about $50\,\mu$T. After start and during deceleration, at propeller rate about 1000 rpm moving sodium is suppressing Earth field hence field inside stays on noise level: $2\,\mu$T. At 1800 – 2000 rpm, depending on temperature, field generation happens and field reaches 0.2 T. No single instrument can cover five decades and variety of sensors is used.

*Fluxgate* – linear range $0 - 350\,\mu$T, in saturated mode useful for pulse counting.

*Different coils* – coils are preferable for inside measurements as they have no temperature correction and for recording spectra as they have enhanced sensitivity

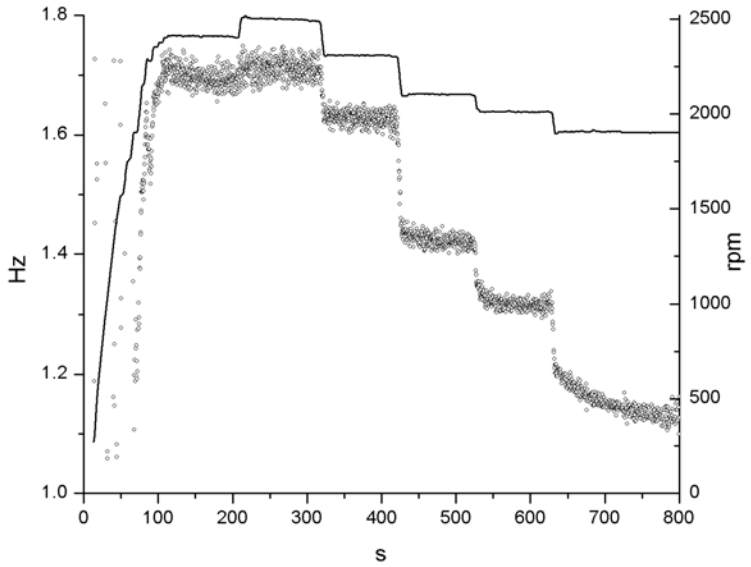


*Fig. 6.* Frequencies follow propeller rotation rate.

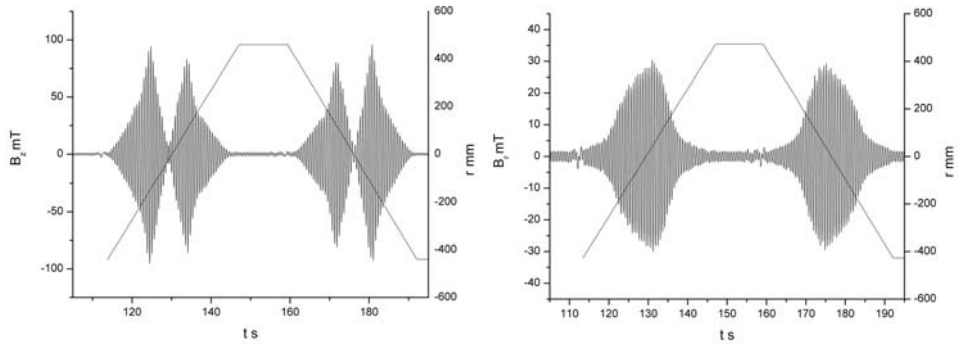


*Fig. 7.* Field records from mobile coils. Left – vertical field, right – radial field.

at high frequencies. Disadvantage – coils are feeling temporary field rate not a field itself. For field recovery we use post-experiment computer Fourier processing.

*Hall sensors* – for outside field measurements. Hall measurements inside were used also. Data were complicated by temperature correction and not considered here.

Inside sensors are located on two levels (left part on Fig. 2). Four upper ports are going inside until the central channel. There are located fluxgate and large size coil used in particular as the reference coil for signal phase determination. On the lower level there is one 12 mm tube going throw the whole device and two side ports. One has 7 mm tip inside the central channel used for spectra measurements. Another is for inserting different instruments directly in the central sodium flow (flow-meter, pressure sensor, etc). In the 12 mm tube we can alter different instruments: array from 15 immobile coils, Hall sensor array and a shuttle with 3 coils aligned orthogonally. The shuttle is moved throw the channel forth and back by a motor.

Outside sensors are Hall sensors. In this paper we report only on commercial 3D Hall sensor moved by a motor vertically along the whole device.

*3.2. Field dependence on rotation rate.* Fig. 3 show vertical ($z$) field dependence on rotation rate recovered from the "reference" coil located on the upper level. Field there has remarkable strength. On three highest rotation rates it has almost no propeller dependence. In the same time frequency (Fig. 6) remarkable follow all rotation steps.

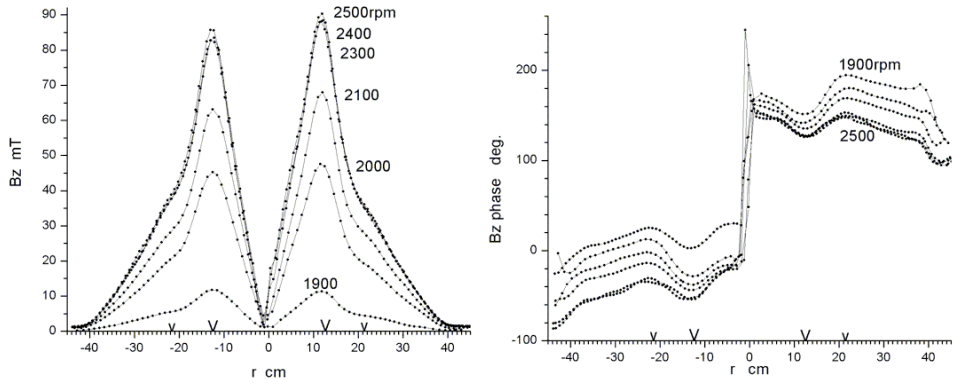


*Fig. 8.* Radial profiles for vertical field. Left – field, right – phase. V and v marks inner wall locations.

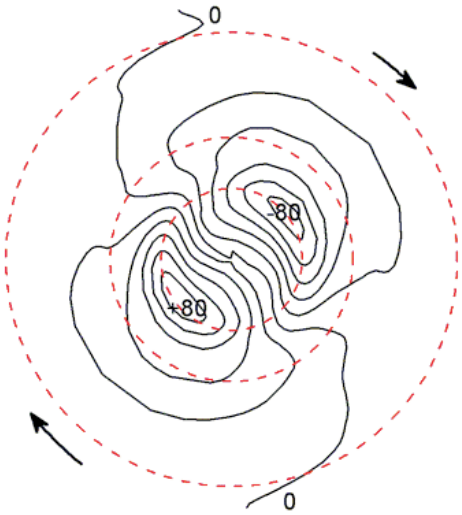


*Fig. 9.* Vertical field pattern rotates in the arrow direction.

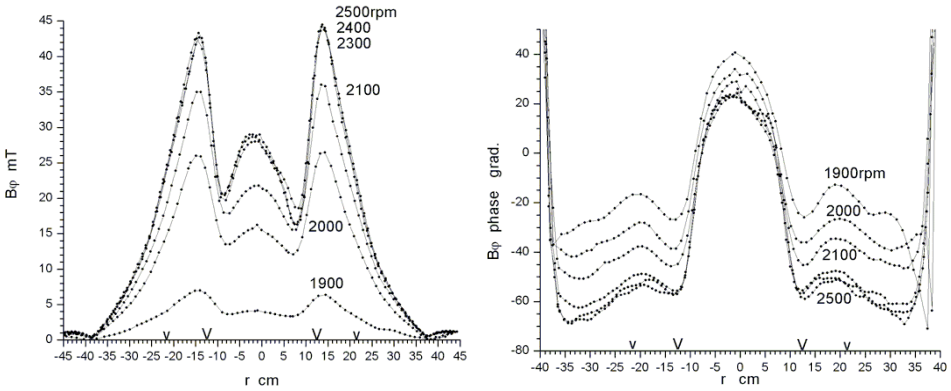


*Fig. 10.* Radial profiles for azimuthal field. Left – field, right – phase. V and v marks inner wall locations.

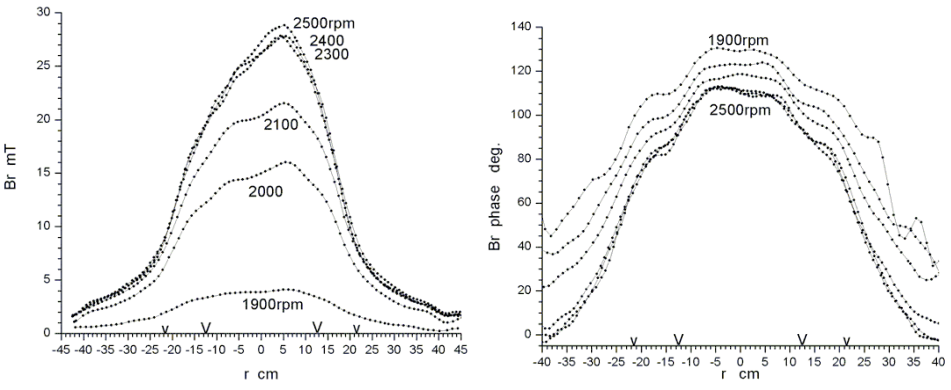


*Fig. 11.* Radial profiles for radial field. Left – field, right – phase. V and v marks inner wall locations.

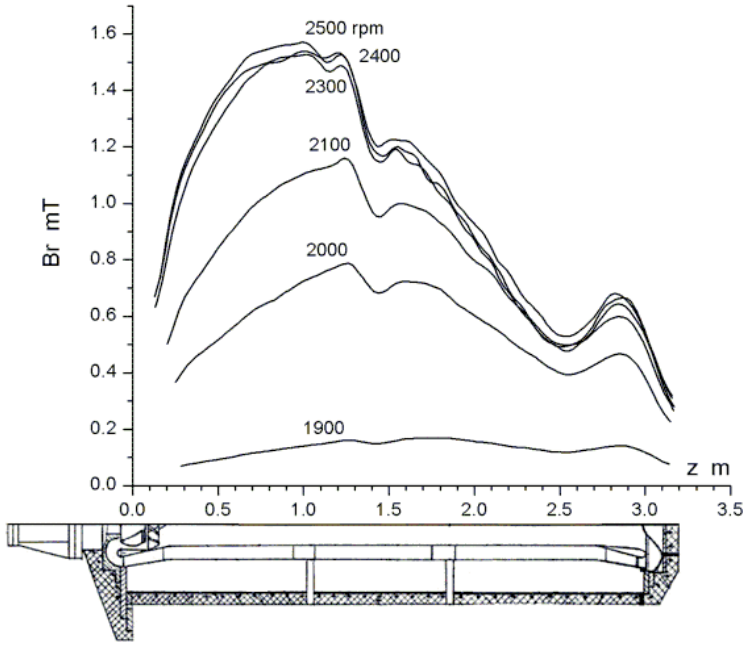


*Fig. 12.* Vertical profiles for radial field.

*3.3. Field radial dependence.* Field radial dependence is measured by means of shuttle based coils. Some fragments from field records together with coil coordinate are presented on Fig. 7. To have comprehensive phase shifts signals are band filtered.

Relaying each peek to the corresponding coordinate we got radial dependence for vertical (Fig. 8*a*), azimuthal (Fig. 10*a*) and radial (Fig. 11*a*) fields. Comparing record zeros with the reference coil zeros we got radial dependences for correspond-

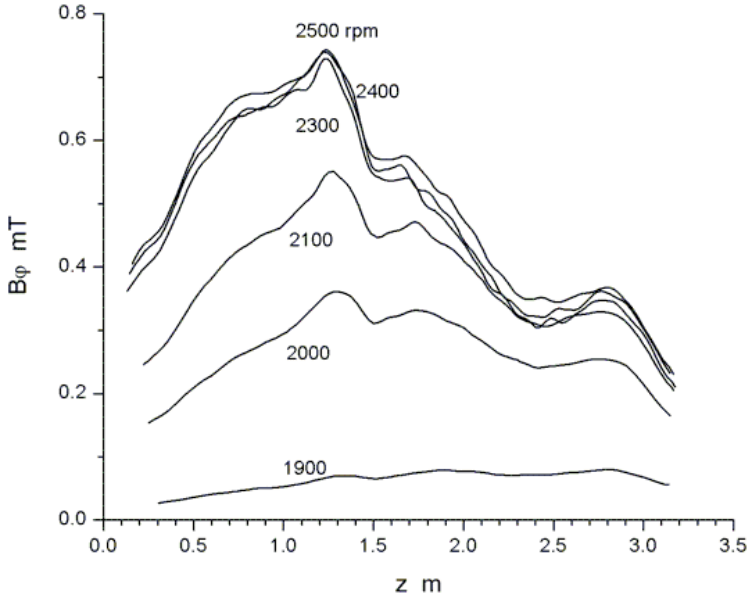


*Fig. 13.* Vertical profiles for azimuthal field.

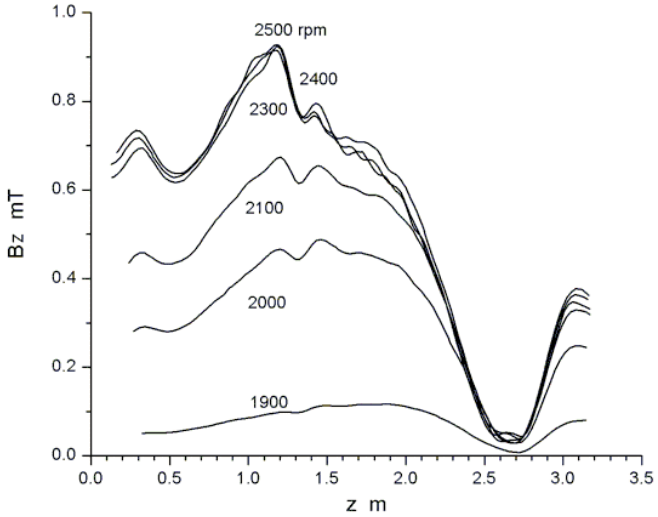


*Fig. 14.* Vertical profiles for vertical field.

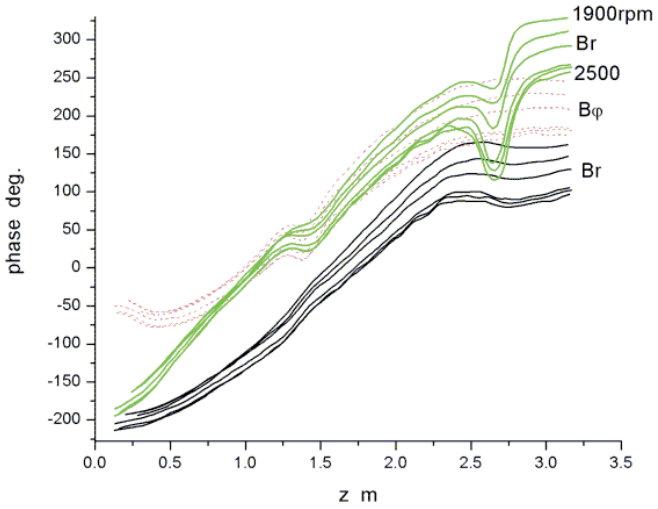


*Fig. 15.* Vertical profiles for phase shift.

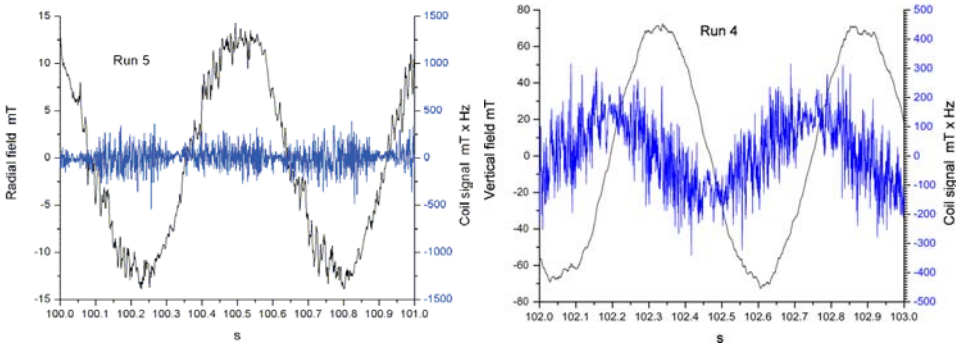


*Fig. 16.* Fragments from two field records. Different small coils at very place but in different time.

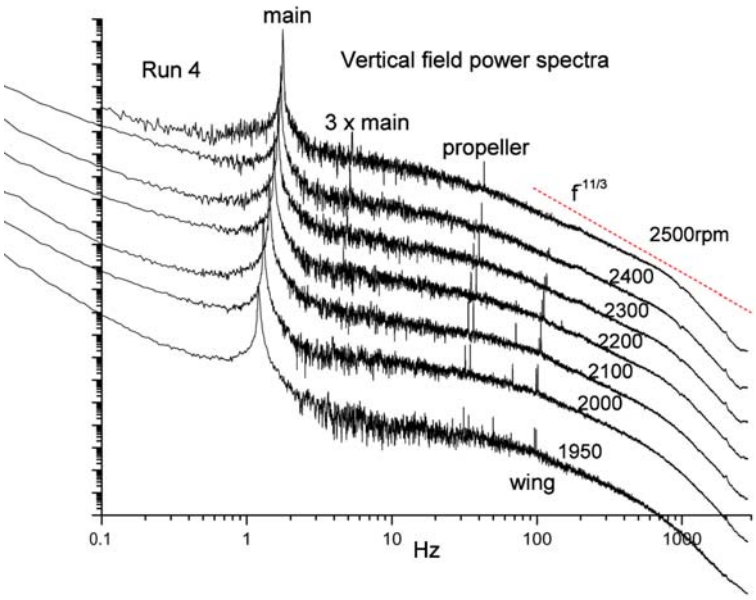


*Fig. 17.* Frequency spectra for vertical field.

ing phase shifts (Fig. 8*b*, Fig. 10*b*, Fig. 11*b*). At last, combining Fig. 8*a* with Fig. 8*b* we got Fig. 9 with level lines for vertical field. Fig. 9 should be understood as a field pattern which rotates in the arrow direction.

In principle all figures Fig. 8 – Fig. 11 should be symmetric to the origin. The visible asymmetry is caused by some angular misalignment of coils. Situation is deteriorated by the fact that the vertical field is much stronger as horizontal one. On Fig. 8 and Fig. 10 correction from post-experiment measured position angle is included. But it is not removing all asymmetry.

*3.4. Field axial (vertical) dependence.* Fig. 12 – Fig. 15 are prepared in the same way as previous ones. Only recorded field is measured by vertically moving

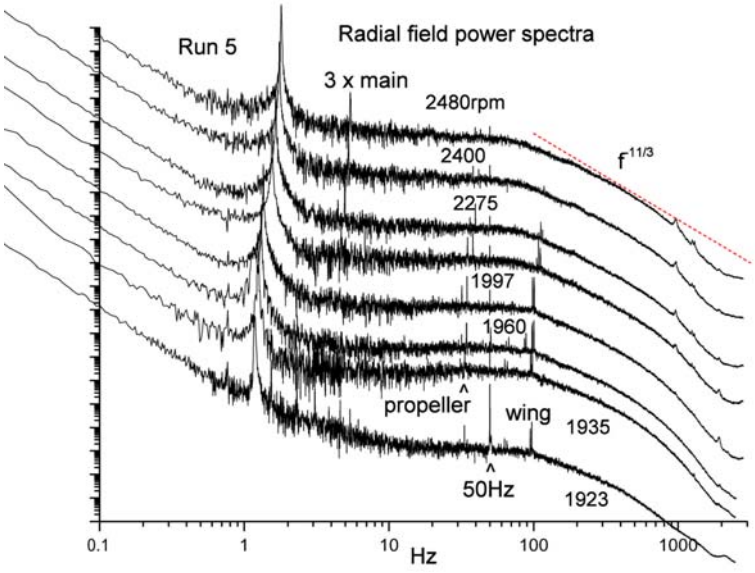


*Fig. 18.* Frequency spectra for radial field at different coil locations.

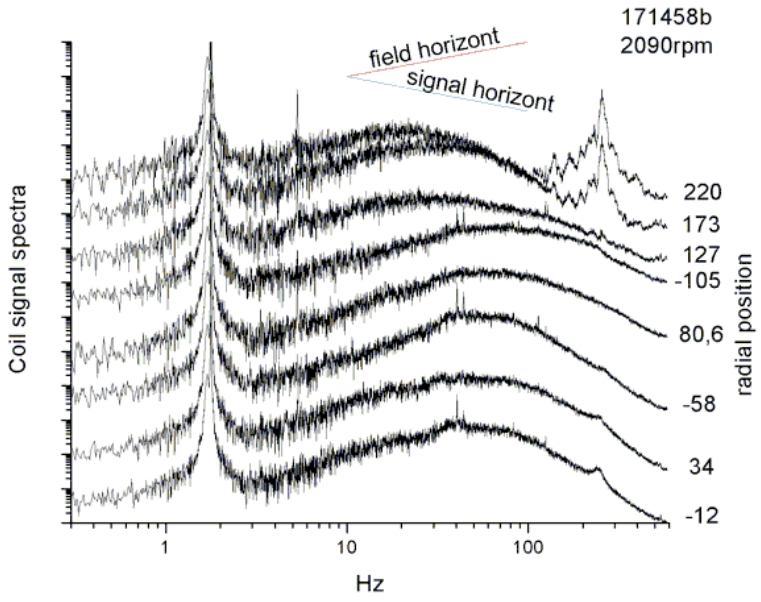


*Fig. 19.* Frequency spectra for radial field at different coil locations.

3D Hall sensor. Pictures show saturation process – with raising rotation rate field in the upper part is raising faster as in the lower one. In the central part phase rates for all three field components are equal. Kink at $z = 1.4$ seems caused by sensor passing near by a horizontally located iron bar.

**4. Magnetic branch of turbulence.** On Fig. 7–15 magnetic field was band filtered. Only principal field was left there, the turbulent details were lost. The real field is rich with turbulent details (Fig. 16). Some of turbulence spectra are presented on Fig. 17, Fig. 18 and Fig. 19. For comparison on Fig. 17 and Fig. 18 is marked the $-11/3$ law (the straight line). So should be magnetic field spectra if turbulent velocities could follow Kolmogorow's $1/3$ rule.